Article

A Method for Defining Sedimentary Characteristics and Distributions and Its Application in Qinnan Depression, Bohai Bay Basin

Zehua Zhang [1], Chunqiang Xu [2], Chenjie Wang [2], Hong Li [2], Wensen Zhu [2], Hongliang Wang [1,*], Kaixuan Liang [1] and Yong Su [1]

1 School of Energy Resources, China University of Geosciences (Beijing), Beijing 100083, China; 3006200026@cugb.edu.cn (Z.Z.); 2106200039@email.cugb.edu.cn (K.L.); 2006200017@email.cugb.edu.cn (Y.S.)

2 Tianjin Branch of China National Offshore Oil Company Ltd., Tianjin 300452, China; xuchq2@cnooc.com.cn (C.X.); wangchj34@cnooc.com.cn (C.W.); lihong31@cnooc.com.cn (H.L.); zhuws@cnooc.com.cn (W.Z.)

* Correspondence: whliang@cugb.edu.cn; Tel.: +86-010-82321865

Abstract: A new method incorporating geophysical analysis and geological analysis is proposed to define the sedimentary characteristics and distributions in basins with few drilling wells to promote the exploration of reservoirs. This method is applied to a study, through which its principles, closed-loop workflow and technologies are introduced in detail and the sedimentary characteristics and distributions of the study area are accurately defined. During the application process of the method, a compatible geological model is established, based on which the seismic data are interpreted and the results derived from the interpretation are further verified via seismic forward modeling. The study results exhibit a successive sand-rich deposition from the retrogradational gully-filling gravity flow deposition including near-shore fans, slope fans and basin-floor fans delimited by different slope break belts in transgressive sequences to the progradational delta deposition in a retrogressive sequence including braided river deltas with a long extension distance and fan deltas developed along a steep slope belt. And the potential reservoirs are located at the point-out sites of sand bodies with lower average P-wave velocities than those of muddy sediments. The proposition and application of this method are of great significance for oil and gas exploration.

Keywords: geological model; seismic facies; paleogeomorphology; stratigraphic pattern; seismic forward modeling; Qinnan depression

1. Introduction

Accurately defining the sedimentary distributions and characteristics in a basin is fundamental for the exploration of oil and gas reservoirs [1–5]. Over the past years, lithofacies and logging and seismic data have been used jointly to recognize the distributions and characteristics of potential reservoirs [6–10], of which the procedures usually include (1) becoming acquainted with the geological setting of the study area and identifying various seismic facies (e.g., external geometry and internal configuration shown in seismic sections) and logging facies mainly indicated by logging curves and (2) converting geophysical facies to sedimentary facies via borehole calibration to define the sedimentary characteristics and distributions. The above process was proven to be a valid method for defining the sedimentary characteristics and distributions, but has its limitations because of the difficulty and high cost of obtaining all types of data in actual exploration. In order to successfully discover reservoirs with few wells in the early exploratory stage, sedimentologists and geophysicists have effectively analyzed seismic data from the aspects of geological recognition and data digitization and visualization [11]. Based on sedimentology, sequence stratigraphy and geomorphology, sedimentologists usually recognize the sedimentary distributions and

characteristics through a comprehensive analysis of the paleogeomorphology (restored via multiple methods such as the residual thickness method, the impression method and the sequence stratigraphic method) [12–14] as well as external geometries (e.g., wedge, lens and fan), internal configurations (e.g., chaotic, parallel and progradational) and reflection termination patterns (i.e., onlap, toplap, downlap and truncation) displayed in seismic sections [15–22]. However, the analysis results of sedimentology primarily obtained via visual observation present uncertainty and non-uniqueness. Geophysicists prefer to focus on seismic data processing, such as phase shifting, the stacking of multiple attributes and the auto-classification of seismic facies [10,23–29]. Many seismic parameters including amplitude, frequency, interval velocity and waveform have been extracted or recalculated to reflect the characteristics and distributions of sedimentary bodies [10,24,28,30–33]. And seismic forward modeling has been used to speculate the seismic reflection features of sedimentary bodies for facilitating the recognition of sedimentary distributions and characteristics [34–40]. Although the reprocessing or modeling of seismic data is conducive to improving data readability and diminishing subjective effects, calculation error and the absence of geological theory can lead to inaccurate analysis results and distort depositional models. Consequently, a method to accurately define the characteristics and distributions of sedimentary bodies with the inadequate drilling data obtained is still required.

A new method integrating geological analysis and geophysical analysis is proposed to resolve the difficulty in accurately recognizing the sedimentary characteristics and distributions in basins with few drilling wells. This study introduces the principle and the workflow of the method in detail by applying the method to a case study on the northern Qinnan depression at the edge of the Bohai Bay Basin to define its sedimentary characteristics and distributions, and sheds light on oil and gas exploration in similar basins with few wells.

2. Geological Setting

The Qinnan depression, the study area, is located at the edge of the Bohai Sea in China with a gross area of approximately 2300 km^2, and is surrounded by the Qinnan uplift, Liushouying uplift, Liaoxi uplift and Shijiutuo uplift. The study area can be divided into the eastern, western and southeastern sags (Figure 1) [40,41]. Among them, the western sag is characterized by a steep slope induced by fault activities, and the eastern sag features a gentle slope. Controlled by the Qinnan I growth fault (F1) and the Qinnan II growth fault (F2), the Qinnan depression has gone through the syn-rift stage (65.0–24.6 Ma) and the post-rift thermal subsidence stage (24.6 Ma–present) [42,43]. The syn-rift stage is further divided into four substages: the strong rift subsidence (65.0–50.5 Ma) during the Paleocene Kongdian formation (Ek), the strong rift subsidence with a weak strike-slip component (50.5–38.0 Ma) from the fourth member of the Eocene Shahejie formation (Es$_4$) to the third member of the Eocene Shahejie formation (Es$_3$), the rift subsidence with a strike-slip component (38.0–30.0 Ma) from the second member of the Eocene Shahejie (Es$_2$) formation to the third member of the Oligocene Dongying formation (Ed$_3$), and the rift subsidence with a strong strike-slip component (30.0–24.6 Ma) (Figure 1d) [44,45].

The lacustrine sediments mainly consist of sandstones and mudstones deposited during the Eocene Shahejie formation (Es) (Figure 1e) [46–48]. The deposits in the Es covered by fluvial deposits constitute important source rocks and reservoirs of the Qinnan depression. Despite the three wells exhibiting low oil development values in the northern Qinnan depression, the amount of oil and gas that was developed from the southeastern sag indicates that the northern Qinnan depression still has potential oil and gas resources today [49]. Therefore, it is of great significance to understand the sedimentary characteristics and distributions of the northern Qinnan depression with little wells.
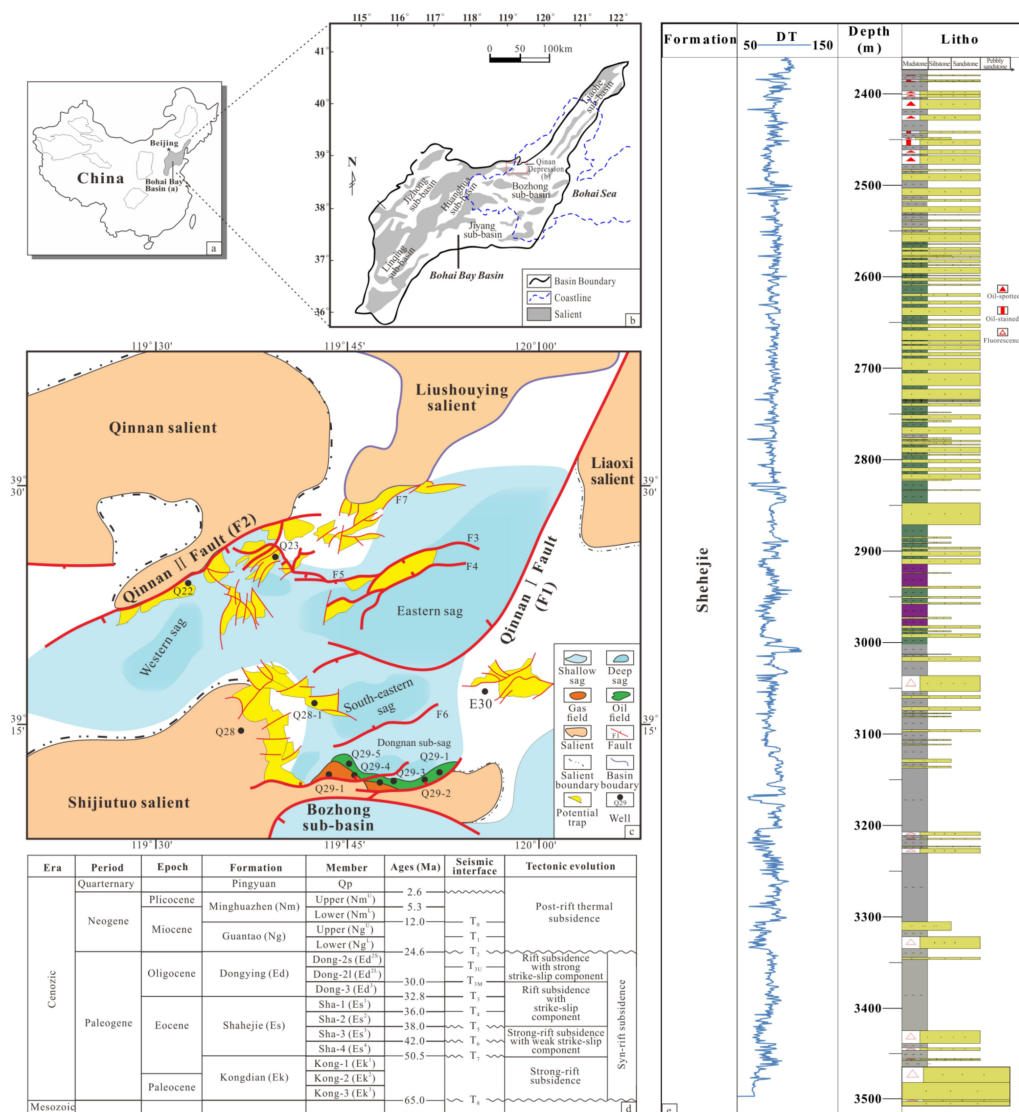
Figure 1. (**a**) Location of Bohai Bay Basin, (**b**) location of Qinnan depression, (**c**) geological framework of the Qinnan depression, (**d**) generalized stratigraphic column and tectonic evolution of the Qinnan depression, and (**e**) lithology and acoustic logging of the Eocene Shahejie formation in Qinnan depression.

Considering that the Es$_3$ is the main hydrocarbon-bearing strata in the Bohai Bay Basin and the Es$_4$ is absent in the eastern sag, the Es$_3$ was chosen for the application of the new method proposed in this study.

3. Data and Method

3.1. Data

A combination of seismic data and logging data of at least one well or a combination of seismic data and acoustic velocities of outcrop is necessary for the utilization of the new method proposed in this paper. Provided by the China National Offshore Oil Corporation Limited (CNOOC), Tianjin Branch, three-dimensional (3D) seismic data, the logging data of one well and the time–depth relation are leveraged in this study. The dominant frequency of 3D seismic data processed by the pre-stack time migration is 35 Hz. Three kinds of software including Landmark, ResForm and Tesseral are used.

3.2. Method

The new method put forward in this paper relies upon the construction of paleogeo-morphology, the analysis of stratigraphic pattern, the interpretation of seismic data and

the verification via seismic forward modeling (henceforth known as the CAIM method). During the application of the CAIM method, all analysis processes follow the principles of sedimentology, sequence stratigraphy and seismic geomorphology. And the interpretation of seismic data revolves around well-recognized criteria which have been summarized in some existing publications [50,51]. The method is to apply the constructed model based on the analysis results of paleogeomorphology and sequence stratigraphy to conduct seismic interpretation, then verify the results of seismic interpretation and, finally, accurately define the sedimentary characteristics and distributions according to the verified seismic interpretation results (Figure 2). The specific steps are as follows:

1. Based on the geological background, choose a suitable method with less workload (e.g., residual thickness) to construct paleogeomorphology for understanding the features and distributions of low-lying areas (gullies), flowpaths and slope break belts.
2. Based on the principle of sequence stratigraphy, establish the stratigraphic framework of the study area to define the stacking pattern of sedimentary bodies in different system tracts.
3. Based on the paleogeomorphic features and the sequence stratigraphic framework of the target interval, modify some existing geological models of basins presenting similar geological settings with the study area to construct a compatible geological model matching the geological characteristics of the study area.
4. According to the seismic interpretation criteria summarized by Veeken et al. (2013) and Xu et al. (2020) [50,51] as well as the compatible geological model, interpret the seismic data using multiple parameters including but not limited to seismic facies.
5. Extract a two-dimensional (2D) sedimentary model from a typical seismic section. And acquire the *P*-wave velocities of different sedimentary bodies from acoustic logging data. Use the constructed velocity model to carry out seismic forward modeling. When the section obtained from seismic forward modeling is consistent with the seismic section, the interpretation of seismic data can be regarded as valid.
6. Based on the interpretation results of seismic data in combination with the plane distribution of sedimentary bodies' peculiar seismic attributes, the sedimentary characteristics and distributions in the target interval of the study area are accurately defined.
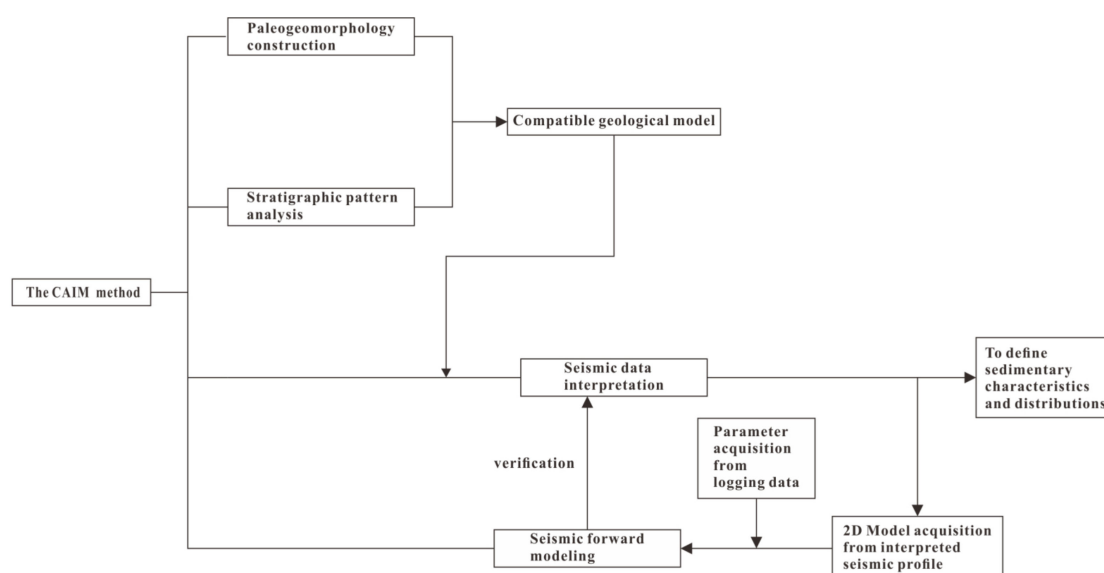

Figure 2. Flowchart of the CAIM method for defining the sedimentary characteristics and distributions.

The application of the CAIM method guarantees the validity of seismic data interpretation and the precision of the descriptions of the characteristics and distributions of potential reservoirs in the study area. Being applied to the study on the Es_3 in the northern Qinnan

depression, the working details of this method are introduced, meanwhile, the sedimentary characteristics and distributions of potential reservoirs in the study area are defined.

4. Application of the Method

4.1. Geological Model

The paleogeomorphic feature and stratigraphic pattern jointly control the sedimentary distribution [52]. Establishing a compatible geological model according to the analysis of the paleogeomorphology and stratigraphic pattern is a precondition of interpreting the seismic data.

4.1.1. Paleogeomorphology Construction

To select the construction method of paleogeomorphology in a study area with few wells, the geological setting should be taken into account. For a depression with a single provenance, the application of sequence stratigraphy with the restoration of denudation is ideal for identifying the flowpaths and depocenters in detail. However, when it comes to multi-provenance depression, it is difficult to restore denudation. In order to identify the flowpaths and local depositional centers swiftly, the application of residual thickness is considered to be effective and convenient.

Restored by using residual thickness, the paleogeomorphology of Qinnan depression before the Es_3 exhibits five high-lying regions, four low-lying regions and multiple slopes (Figure 3a). The sediments in the western low-lying region corresponding with the western sag source from the Qinnan and Shijiutuo uplifts and the sediments in the middle low-lying region near the Q23 well and in the eastern low-lying region corresponding with the eastern sag are primarily sourced from the Liushouying uplift (Figures 1 and 3a). Seven drainages are distinguished by six watersheds. The drainage originating from the Qinnan uplift has two trends: a northeast–southwest direction and a near north–south direction. The three northeast–southwest trending flowpaths divided by four watersheds imply that there are three sedimentary bodies at least in the middle low-lying region. Different from the middle low-lying region, the north of the eastern low-lying region is divided into three drainages by two watersheds. Among them, the altitude of the western drainage is higher than the others, which suggests that the sediment deposition in the western drainage formed after the other two drainages were filled up. Additionally, the trends of six gullies in three drainages of the eastern low-lying region indicate four near north–south trending and northeast–southwest trending flowpaths (Figure 3a), which represents the axial direction of sedimentary bodies.

The faults and topographic flexures jointly result in the formation of multiple slope break belts, which control the accommodation change and affect the location of the local sedimentary centers. In the Qinnan depression, step-fault slopes are the main type of slopes, including multi-level step-fault gentle slopes in the eastern sag and step-fault steep slopes in the western sag (Figure 3). Three distinct slope break belts result in three local low-lying regions (Figure 3b). Among them, the first-order slope break belt near the northern source areas is caused by the fault and topographic flexures. The drop of the western first-order slope break belt is higher than that of the eastern first-order slop break belt. The second-order slope break belt is mainly brought about by faults, of which the fault amplitude in the middle low-lying region is much higher than that in the eastern sag. The third-order slope break belt with a high drop corresponding to the F3 fault and the steep slope fault belt caused by the F1 fault jointly result in the formation of the subsiding center of the eastern sag (Figure 3b).
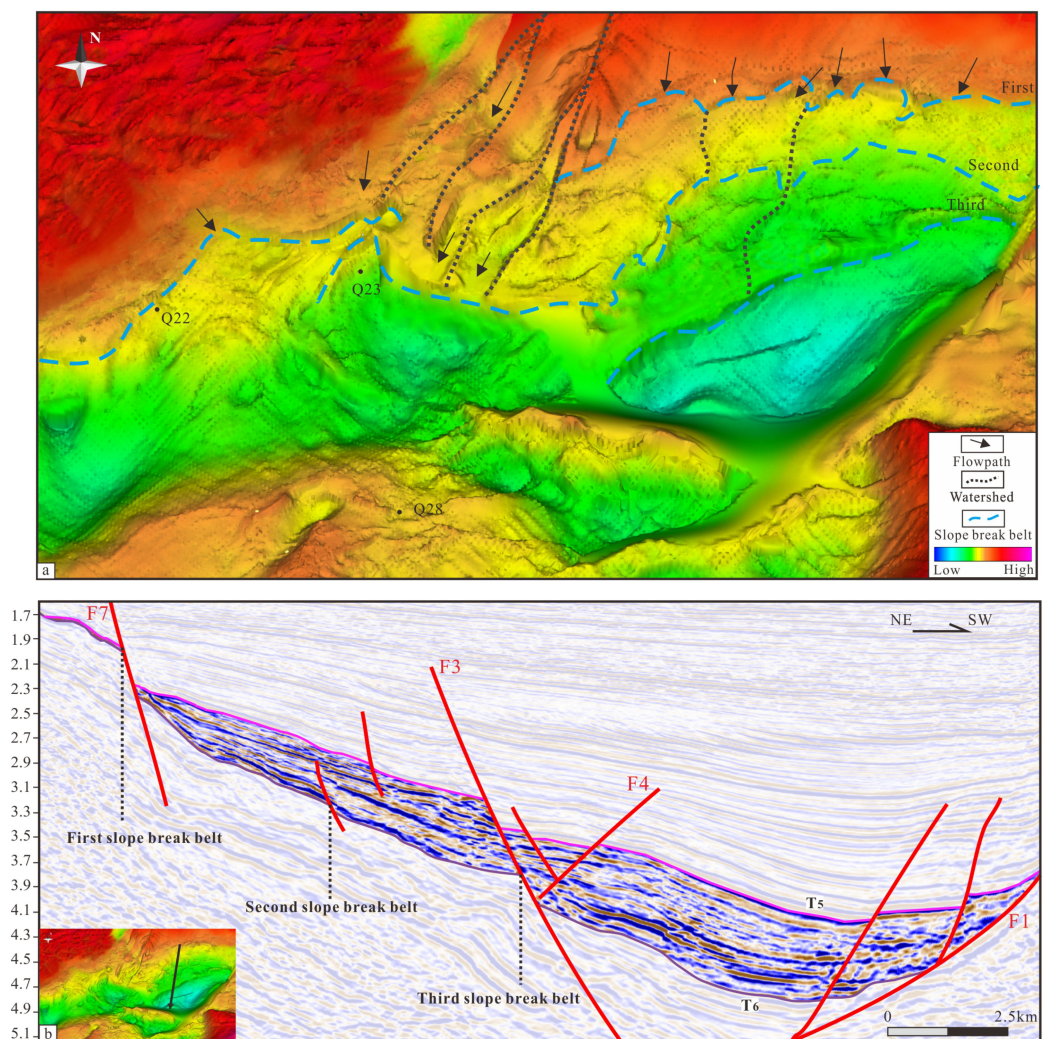
Figure 3. (**a**) The paleogeomorphic map before the third member of Eocene Shahejie formation (Es₃) in Qinnan depression. (**b**) A seismic section showing topographic features of the bottom of the Es₃ and three slope break belts in the Es₃.

In general, the flowpaths indicated by the trends of the gullies and local low-lying regions influenced by multi-level slope break belts suggest that sedimentary bodies fill up the local low-lying regions in the early stage of the Es₃ and have north–south and northeast–southwest trends in the Qinnan depression.

4.1.2. Stratigraphic Pattern

The stratigraphic pattern consists of a sequence stratigraphic framework and its internal depositional configuration [15]. The establishment of the sequence stratigraphic framework is the key for predicting the characteristics and distributions of sedimentary bodies. The Es_3 is divided into the upper sequence (Es_{3U}) and the lower sequence (Es_{3L}) by identifying three sequence boundaries and one maximum flooding surface. The Es_{3U} is thicker than the Es_{3L}. The T_6 and T_5 sequence boundaries correspond to the bottom surface and top surface of the target interval, respectively, which are identified on the seismic reflections via truncation and the toplap below them as well as the onlap above them; the T_{6M} sequence boundary is the bottom boundary of the Es_{3U}, and is characterized by the onlap above it; and the maximum flooding surface (MFS) of both the Es_3 and Es_{3U} is a downlap surface, which divides the Es_{3U} into two system tracts including the lowstand to the transgressive systems tract (LST and TST) and the highstand systems tract (HST) (Figure 4). The T_{6M} and MFS surfaces both terminate on T_6 between the first-order slope

break belt and the second-order slope break belt (Figure 4). Therefore, the Es_{3L} and the LST and TST of the Es_{3U} distribute in the south of the first-order slope break belt.
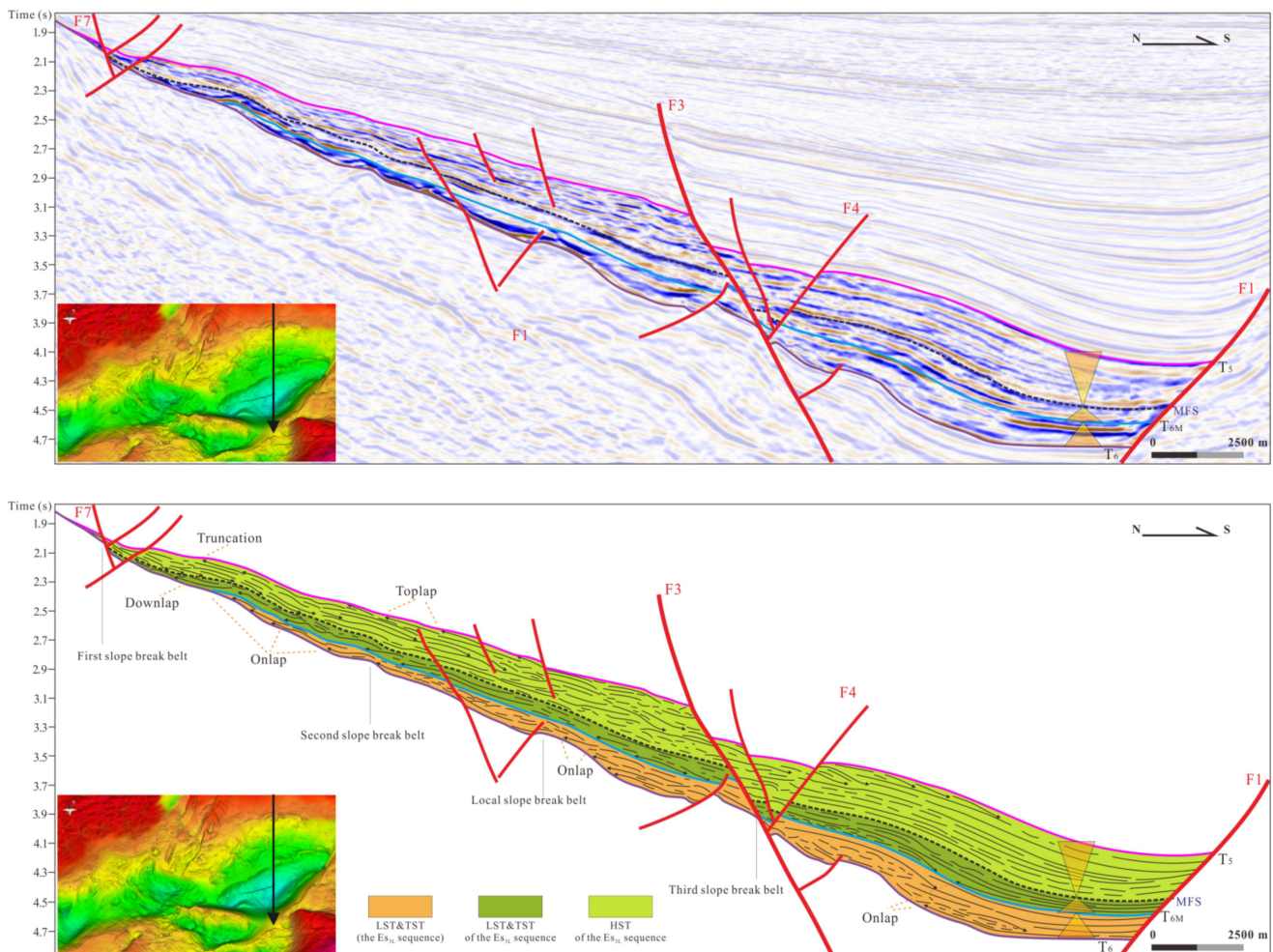

Figure 4. The sequence stratigraphic framework of the Es_3 in Qinnan depression.

The absence of progradation reflection in the upper Es_{3L} implies that the HST is not developed. The retrogradation reflection in the Es_{3L} indicates the rise in the base level (Figure 4). Three lentoid sedimentary bodies with chaotic reflections or chaotic/hummocky reflections fill up the low-lying lands (relatively high accommodation) induced by different slope break belts in dip sections (Figure 4), which signifies subaqueous deposits in different locations of the slope. The onlap spot of the seismic reflection axes gradually moves to the top of the slope, indicating retrogradation and transgression in the Es_{3L}. A local high accommodation indicated by the thickening of sequences is always accompanied by the development of faults crossing the Es_{3L} (Figure 4), suggesting that the development of faults occurs before the formation of the Es_{3L}.

The LST and TST are thinner than the HST in the Es_{3U} sequence. Inheriting from the Es_{3L}, three slope break belts lead to the formation of areas with a relatively high accommodation in the LST and TST of the Es_{3U} (Figure 4). Hummocky reflections with a weak to medium amplitude are present between the first-order slope break belt and the second-order slope break belt as well as between the third-order slope break belt and the F1 fault; clean blocky reflections with a weak amplitude are shown between the second-order slope break belt and the F3 fault (Figure 4). Similar to the Es_{3L}, faults crossing the LST and TST of the Es_{3U} induce the increase in local accommodation, indicating that the faults develop before the formation of the LST and TST of the Es_{3U}. The bidirectional onlap reflection is observed in local low-lying regions occasionally. The characteristics of the

seismic reflections in the LST and TST the Es$_{3U}$ are similar to those in the Es$_{3L}$, indicating the filling of the gullies, the retrogradation of the sedimentary bodies and transgression. Convergent progradational seismic reflection axes with a medium amplitude are shown in the HST, which suggests the progradation of sedimentary bodies and a decreasing accommodation (Figure 4). The sedimentary pattern in the HST is less influenced by slope break belts. Different from the LST and TST of the Es$_{3U}$, faults crossing the HST do not lead to the thickening of sequences (expect for the F7, F3 and F1 faults), which indicates that the faults develop after the formation of the HST and have little influence on the sedimentary characteristics of the LST and TST of the Es$_{3U}$ (Figure 4). The development of the F7, F3 and F1 faults induce the formation of slope break belts and increase the thickness of the sequences in the Es3. Therefore, the F7, F3 and F1 faults develop before the formation of the Es$_3$ and control deposition in the Qinnan depression.

Based on the sequence stratigraphic framework, the vertical sedimentary pattern of the Es$_3$ includes a successive stacking of retrogradational sedimentary bodies indicated by filled gullies from the Es$_{3L}$ to the LST and TST of the Es$_{3U}$ and overlying progradational sedimentary bodies in the HST of the Es$_{3U}$. The faults control the change in the topography and the sequence thickness. The growth of the F1 fault causes the formation of the Qinnan depression and an eastern gentle slope [44,45]. Thus, it is inferred that the F1 fault, as a synsedimentary fault, controls the change in the accommodation and topography and, in turn, controls the distribution, amount and characteristics of sequence stratigraphy.

4.1.3. Compatible Model

The geological model's high applicability tends to lead to the seismic interpretation's high accuracy. Basins with similar geological settings usually have similar geological models. Therefore, the existing geological models of basins with a geological setting similar to that of the study area can be drawn upon after certain modification to produce the geological model of the study area. Drawing upon and modifying existing geological models of sedimentary basins with similar geological settings to establish a compatible geological model by leveraging the sequence stratigraphic framework and paleogeomorphic features of the study area is a key procedure of the CAIM method proposed in this paper, which will facilitate seismic data interpretation and further improve the validity of the sedimentary characteristics and distributions.

Up to now, a lot of geological models of the sags or depressions of rift basins have been established [51], which present retrogradational clinoforms in the LST and TST and progradational sand bodies in the HST. Based on the paleogeomorphic features and sequence stratigraphy of the Es$_3$ in the Qinnan depression, a compatible geological model modified from some existing depositional models of other depressions in the Bohai Bay Basin (a rift basin) is established (Figure 5). The flowpaths indicated by the trends of the gullies suggest that the axial direction of the sedimentary bodies is mainly from the northeast to the southwest. Under the MFS, two sets of sedimentary bodies in two transgressive sequences are predicted, which, respectively, incorporates three sedimentary bodies filling up three low-lying lands controlled by three slope break belts. In view of the tectonic evolution in the Es$_3$ and the gully-filling seismic facies without progradation reflections, the three sedimentary bodies of one set can be regarded as subaqueous gravity flow deposits and are divided into near-shore deposition near source areas, slope deposition between the first-order and second-order slope break belts and basin-floor deposition in the subsiding center. The progradation reflections overlying the MFS converge on the center of three low-lying regions (Figures 3 and 5), indicating the progradational sedimentary bodies with a gradually falling base level.
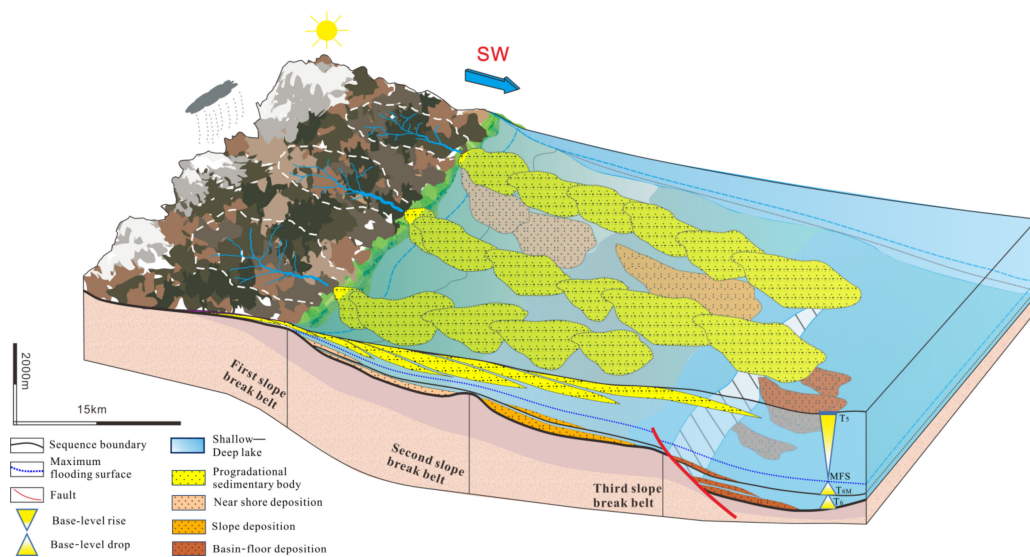
Figure 5. A compatible geological model suggested by the sequence stratigraphic framework and paleogeomorphic features.

4.2. Seismic Interpretation

Using seismic parameters to analyze lithology and sedimentary facies is crucial for defining the sedimentary characteristics and distributions of a study area [11]. With the development of computer science and technology, scholars are more willing to interpret seismic data by reprocessing multiple seismic parameters than by using the view of geology [9,20]. By contrast, the CAIM method highlights the conversion from seismic data to geological messages through the interpretation of seismic data according to a compatible geological model and the extraction of seismic attributes. Based on the geological model established in this study, the seismic facies analysis, as a primary unit of the seismic interpretation section of the CAIM method, is leveraged to define the sedimentary characteristics and distributions of the Es$_3$ in the Qinnan depression. Xu et al. (2020) [51] provided criteria for the interpretation of seismic facies in the Bohai Bay Basin, which are used in this study to interpret the seismic data of the Qinnan depression in the Bohai Bay Basin.

4.2.1. Facies

Six sedimentary facies have been identified by the positions and system tracts of sedimentary bodies and seismic features such as the amplitude, internal configurations and external geometries exhibited in seismic sections. The six sedimentary facies involve braided river delta, fan delta, near-shore subaqueous fan, slope fan, basin-floor fan and lake (Figure 6). Apart from the lake facies, other sedimentary facies are dominated by sandstones. As the fan delta, braided river delta and subaqueous gravity flow deposition are in the shape of a lens with a chaotic or stratiform reflection in the off-axis seismic sections, the sedimentary facies are distinguished through seismic features shown in the along-axis sections rather than in the off-axis sections.

Being observed in the HST of the Es$_{3U}$, the wedged progradation reflection in the dip sections indicates delta deposition. In the Qinnan depression, the fan delta and braided river delta are distinguished by different seismic features and development locations. Characterized by a sigmoid progradation reflection with a medium to strong amplitude, the braided river delta develops at the gentle slope of the eastern sag. The stratiform seismic reflection axis in the braided river delta indicates a successive deposition of the interbedded sandstones and mudstones (Figure 6). As opposed to the braided river delta, the fan delta is developed at the steep slopes caused by fault activities in the western sag, with the high accommodation caused by fault activities, providing a favorable geological setting for its development. In the dip seismic sections, the wedged fan delta with an

overall progradation reflection is indicated by the weak stratiform or chaotic reflection with a weak amplitude (Figure 6), confirming that the fan delta is characterized by thick sandstones and sandy deposits interbedded with muddy deposits.
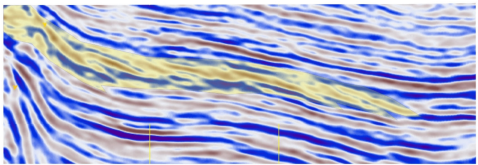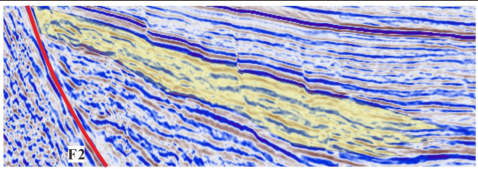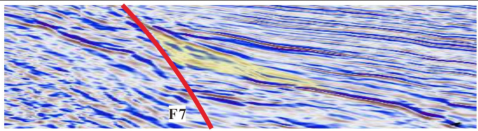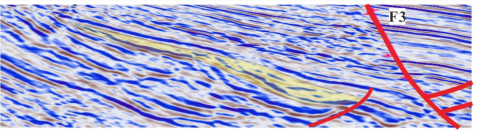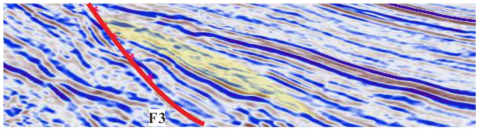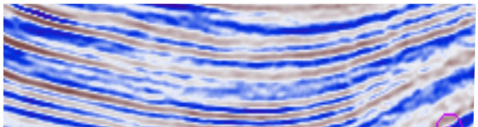
Sedimentary Facies		Position	Examples	System Tract	Seismic Features	Seismic Lithofacies
Braided river delta		Relatively gentle slope		HST	Wedged and lentoid in along-axis and in off-axis seismic sections, respectively; stratiform, medium to strong amplitude, sigmoid prograding clinoform reflections.	Dominated by sandstones
Fan delta		Steep break slope	F2	HST	Wedged and lentoid in along-axis and in off-axis seismic sections, respectively; stratiform or chaotic, weak amplitude, hummocky, prograding reflections	Dominated by sandstones
Subaqueous gravity flow	Near shore subaqueous fan	Near-source slope (Mainly below first slope break belt)	F7	LST & TST	Wedged, lentoid or concave (gully-filling) in seismic sections; chaotic or chaotic-hummocky, weak to medium amplitude reflections which are surrounded by parallel, medium amplitude and continuous seismic reflection	Dominated by sandstones
	Slope fan	Slope (below second slope break belt)	F3			
	Basin-floor fan	Basin floor (below third slope break belt & near the F1 fault)	F3			
Lake		Mainly in subsiding center or the area with low deposition rate		LST & TST & HST	Sheet; parallel, medium amplitude, smooth and continuous reflections	Mudstones or Shales

Figure 6. The distinctive seismic features, development positions, dominated system tracts and seismic lithofacies of different sedimentary facies in the Es$_3$ of Qinnan depression. All examples derive from the northeast–southwest seismic sections.

Wedged, lentoid or gully-filling chaotic reflections with a weak to medium amplitude in along-axis sections indicate inhomogeneous subaqueous gravity flow deposition dominated by sandstones in the Es$_{3L}$ and in the LST and TST of the Es$_{3U}$ in the Qinnan depression (Figures 6 and 7). The weakly continuous retrogradation reflection is present in different types of subaqueous gravity flow deposits. Depending on the location, the subaqueous gravity flow deposits surrounded by continuous reflections are divided into three facies, i.e., near-shore subaqueous fan developing from the top of the slope, the slope fan at the slope controlled by the second-order slope break belt and the basin-floor fan terminating at the bottom of the slope (Figures 3 and 5–7).

The smooth, continuous parallel reflection with a medium amplitude indicates lake facies dominated by mudstones or shales, and represents continuous and stable deposition with a low deposition rate. The parallel reflection indicating muddy deposits in the lake widely exists in all sequences of the Es$_3$ in the Qinnan depression, which usually overlies the subaqueous gravity flow deposition with a lentoid chaotic reflection and underlies the delta deposition with a progradation reflection.
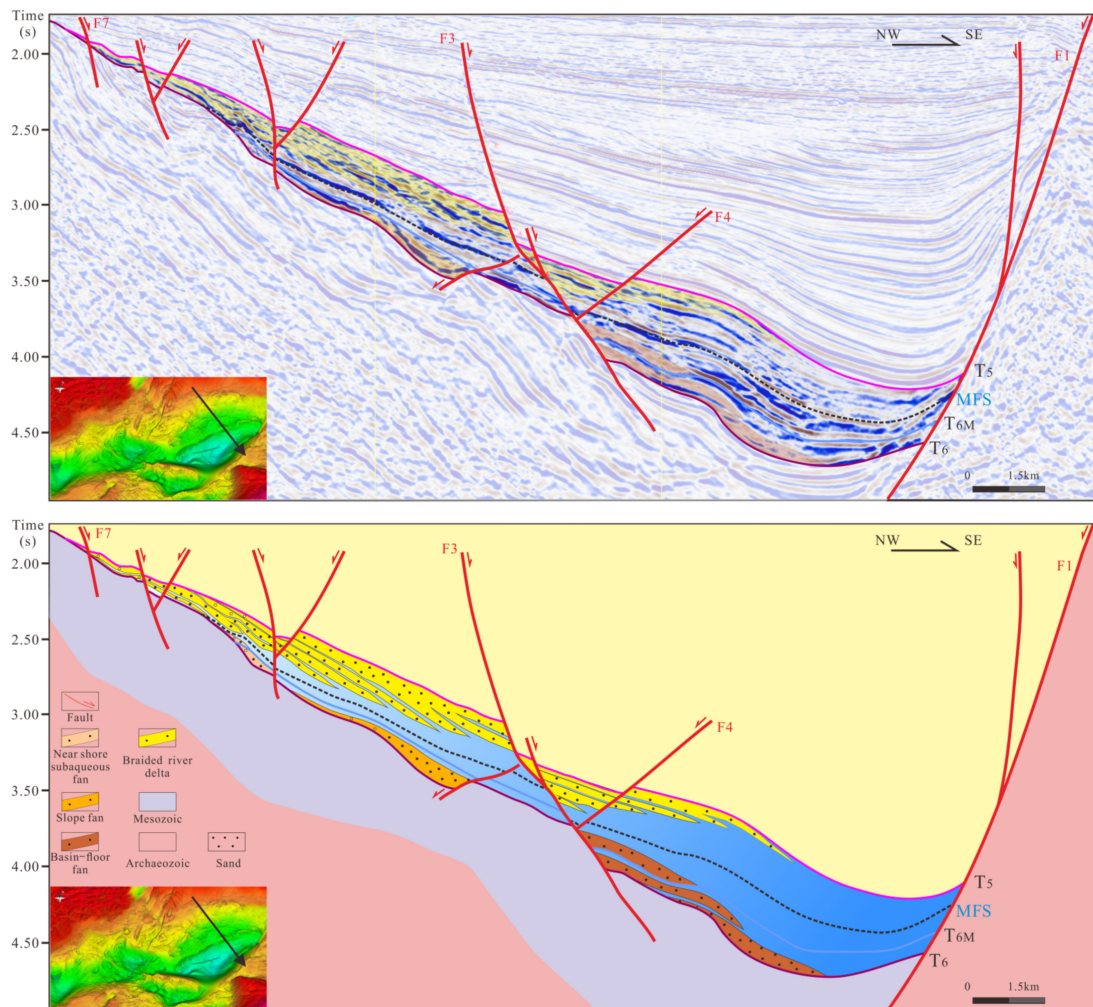
Figure 7. The longitudinal distribution of different sedimentary facies dominated by sandstones in the Es$_3$ of Qinnan depression.

4.2.2. Facies in Section

Seismic sections reflect the vertical stacking of different sedimentary bodies, of which the analysis is fundamental for defining the sedimentary characteristics and distributions. Referring to the compatible geological model, the seismic sections of the Qinnan depression are interpreted according to the configuration of seismic facies that indicate sedimentary facies.

In seismic sections, a continuous parallel reflection of the lake facies represents a muddy deposition and suggests that lithological changes between sandstones and mudstones generally induce an abrupt increase in the amplitude; thus, a continuous parallel reflection with a relatively strong amplitude in a wedged or lentoid sedimentary body signifies mudstone interlayers, which can distinguish sand-rich portions from mud-rich portions in a sedimentary body. In the interpretation of sedimentary facies, corresponding the sand-rich portion of a sedimentary body to sedimentary facies can improve the accuracy of the exploration (Figure 7). In the Qinnan depression, the retrogradational basin-floor fan and the retrogradational near-shore subaqueous fan, both with chaotic reflections in a transgressive sequence represented by the Es$_{3L}$ and the LST and TST of the Es$_{3U}$, are developed from the third-order slope break belt to the F1 fault and from the first-order slope break belt to the second-order slope break belt, respectively (Figure 7). Influenced by faults, the wedged reflection of the near-shore subaqueous fan and of the basin-floor fan converges southward to the sequence boundaries (Figure 7). The slope fan with a chaotic/hummocky reflection only develops in the Es$_{3L}$ from the second-order to the third-order slope break belts, of which the wedged reflection converges northward to

the sequence boundaries and reflects a gully-filling deposition (Figure 7). Overall, slope break belts result in a relatively high local accommodation to form subaqueous gravity flow deposits. The MFS, indicating a widely spread mudstone layer, covers all the subaqueous gravity flow depositions. The progradational sand-rich delta deposition above the MFS extends to the center of the low-lying regions (the depocenter of sags in Qinnan depression) and converges on the T_5 boundary, of which the average thickness is thicker than that of the subaqueous gravity flow deposition.

Generally speaking, the seismic sections show a successive deposition from the retrogradational gully-filling gravity flow deposition delimited by different slope break belts in a transgression sequence to the progradational delta deposition with a long extension distance (Figure 7). During the Es_{3L} and the LST and TST of the Es_{3U}, the faults control the change in the local accommodation and, in turn, control the distribution of the gravity flow depositions. The F1 fault controls the distribution of the subsidence center with a high accommodation, and thus, determines the sedimentary facies types in the subsidence center and their distribution. During the HST of the Es_{3U}, the weakening F1 fault activities induce the decrease in the relative accommodation and, in turn, promote the development of delta facies and influence their distribution.

4.3. Verification

Seismic forward modeling has been widely used to probe the characteristics of reservoirs, verify seismic inversion algorithms and provide guidelines for seismic interpretation [32,37,38]. Apart from that, seismic forward modeling as a part of the CAIM method can also be used to verify the results of seismic interpretation to ensure the accuracy of the sedimentary characteristics and distributions. The attainment of a velocity model from a representative seismic section showing the sedimentary characteristics and distributions of the study area is the key for the utilization of seismic forward modeling. The verification mainly consists of four steps: (1) extract a sedimentary model in depth domain from a representative seismic section displaying sedimentary characteristics and distributions, and establish a typical velocity model by obtaining the *P*-wave velocity (Vp) of different rocks on buried depth from the logging data; (2) set up the framework of seismic forward modeling incorporating the seismic source parameter, source signal and seismic observation system; (3) process point-shot records via gathering, normal move out (NMO), stacking and migration to attain a synthetic seismic section; and (4) compare the synthetic seismic section with the actual seismic section to verify the correctness of the seismic interpretation. It is worth noting that the framework set in step (2) should be as similar to the framework of the seismic data acquisition as possible, and that the processing of the point-shot records must be in accordance with the processing of the actual seismic data.

The seismic interpretation in the Qinnan depression is verified by seismic forward modeling. A seismic section in the eastern sag is selected in the first place, which exhibits representative sedimentary characteristics and distributions including the retrogradational subaqueous gravity flow deposition with a chaotic/hummocky reflection in transgressive sequences, the progradational delta deposition with progradation reflection in regressive sequences and the muddy deposition indicated by a parallel reflection (Figure 7). This section in time domain is interpreted as a sedimentary model in depth domain by the relationship between depth and time as follows:

$$\text{depth (m)} = -1.5661 \text{ time (ms)} + 706.71 \tag{1}$$

Based on the extracted sedimentary model and the relationship between the *P*-wave velocities obtained from the logging data of well Q23 and the burial depth (Figure 8), the sedimentary velocity model is established for simulation (Figure 9a), during which it is scaled down to half its original size to prevent the distortion of velocity assignment. The spot interval, geophone interval (trace interval) and spatial sampling are set as 30 m, 10 m and 4 ms, respectively. The resolution of the seismic data is usually one-quarter of the dominant wavelength (λ); therefore, the source signal is set as zero-phase Riker with a peak

frequency of 70 Hz according to the seismic data's dominant frequency of 35 Hz and the 280 average ratio of the sand-rich sedimentary bodies' Vp to thickness ($\lambda/4$). Given that the actual seismic sections are obtained by the processing (i.e., gathering, NMO, stacking and pre-stack time migration) of the original seismic data, the point-shot records attained from seismic forwarding modeling are also processed in the same way to produce the synthetic seismic section corresponding to the sedimentary velocity model (Figure 9b).
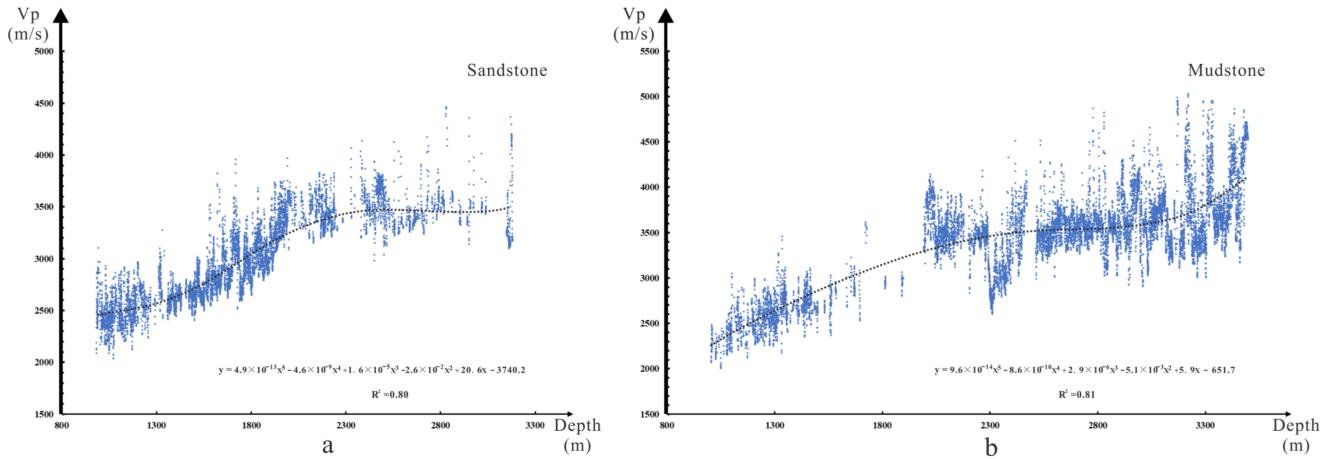

Figure 8. Dependence of rocky *P*-wave velocity on buried depth in northern Qinnan depression. In this figure, y is the rocky *P*-wave velocity (Vp) and x is the depth. (**a**) Dependence of the Vp of sandstone on buried depth. (**b**) Dependence of the Vp of mudstone on buried depth.
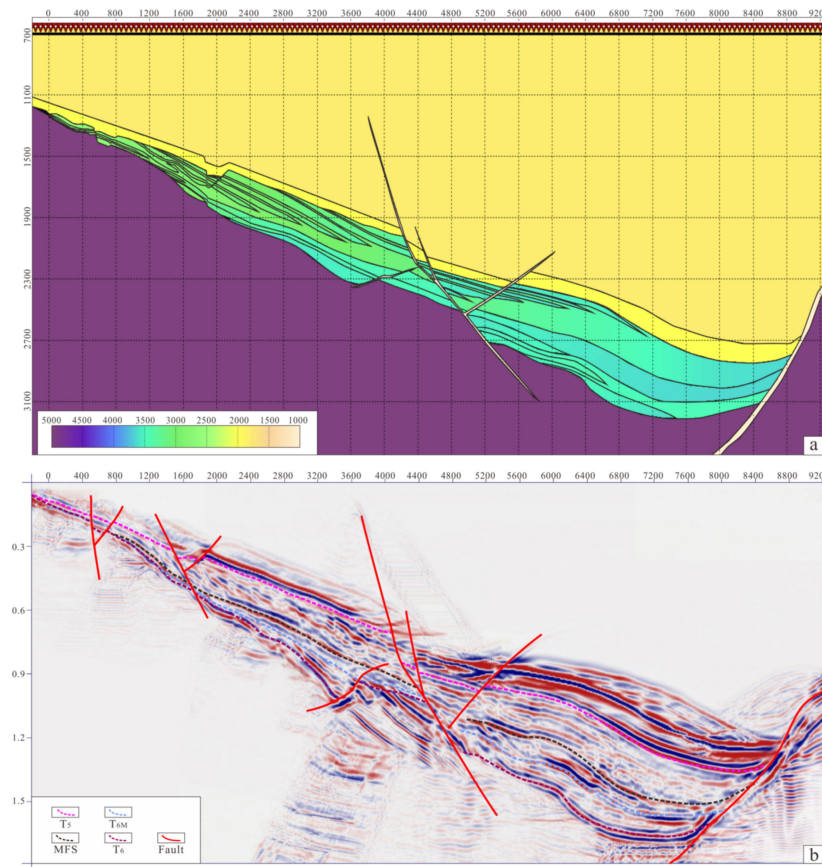

Figure 9. (**a**) A sedimentary velocity model extracted from the typical seismic section shown in Figure 7. (**b**) The synthetic seismic section produced via seismic forwarding modeling.

The synthetic seismic section obtained via seismic forwarding modeling is similar to the actual seismic section (Figures 7 and 9b), suggesting that the results derived via seismic data interpretation are correct. As a result, the understanding of the sedimentary characteristics and distributions in the study area is facilitated, and the exploration accuracy is enhanced.

4.4. Distribution

The CAIM method focuses on recognizing the distributional features based on the correct interpretation of results verified by the simulation and the distribution of extracted attributes that indicate sedimentary bodies so as to accurately define the sedimentary distribution and discover potential reservoirs in a study area.

Representing the lithofacies' transition surfaces, the peak reflection and trough reflection are, respectively, regarded as the interface from low to high impedance and the interface from high to low impedance [53]. Thus, it is most appropriate to leverage the maximum-peak amplitude to distinguish sand-rich deposition from mud-rich deposition, and then to depict the plane distribution of the sand-rich deposition. Based on the average thickness of sedimentary bodies in different sequences, the attribute extractions are compiled by extracting maximum-peak amplitudes from a -20 ms window above the T_6 boundary, a -15 ms window above the T_{6M} boundary and a $+50$ ms window below the T_5 boundary to understand the distribution of the gravity flow deposition in the Es_{3L}, the LST and TST of the Es_{3U} and the distribution of the delta deposition in the HST of the Es_{3U}. The scopes of the sedimentary bodies are indicated by the areas with value anomalies of maximum peak in the plane maps (Figure 10). In general, the distributional area of the sedimentary bodies decreases firstly and then increases from the Es_{3L} to the HST of the Es_{3U}.

In the HST of the Es_{3U}, multiple progradational braided river deltas with three flow-paths cover almost the entire northern Qinnan depression. Five interconnected braided river deltas with the near north–south flowpath develop in the eastern sag, of which the in-flow mounds are closely related to the development of gullies; three interconnected braided river deltas with the northeast–southwest flowpath are present in the middle low-lying region and connect with a fan delta in the north; three progradational braided river deltas with the southwest–northeast flowpath fill in the western sag, which is suggested by the lentoid reflection below the T_5 boundary and the extracted maximum-peak amplitude map; and four fan deltas sourced from the Qinnan uplift are arranged along the Qinnan II fault (F2), of which the tail end connects with the braided river deltas (Figures 3 and 10a,b).

In the LST and TST of the Es_{3U}, four near-shore subaqueous fans are arranged along the first-order slope break belts. Multiple slope fans of the northeast–southwest trend are found in the middle low-lying region, of which the distribution is controlled by the second-order slope break belt and gullies. Five basin-floor fans are deposited in the depocenter of the eastern sag, which are delimited between the third-order slope break belt and the F1 fault (Figure 10c,d).

The subaqueous gravity flow deposition has a larger area in the Es_{3L} than in the LST and TST of the Es_{3U}. Three slope break belts limited the distribution of subaqueous gravity flow deposition in the eastern sag (Figure 10e,f). The western slope break belt with a high drop mainly controls the formation of the Es_{3L} of the Qinnan depression, which provides a favorable geological setting for the development of four slope fans filling up the low-lying lands in the eastern sag and of three near-shore subaqueous fans filling up the middle low-lying region (Figures 3 and 10). Additionally, there exists interconnected slope fans sourced from the Shijiutuo uplift (Figure 10f).
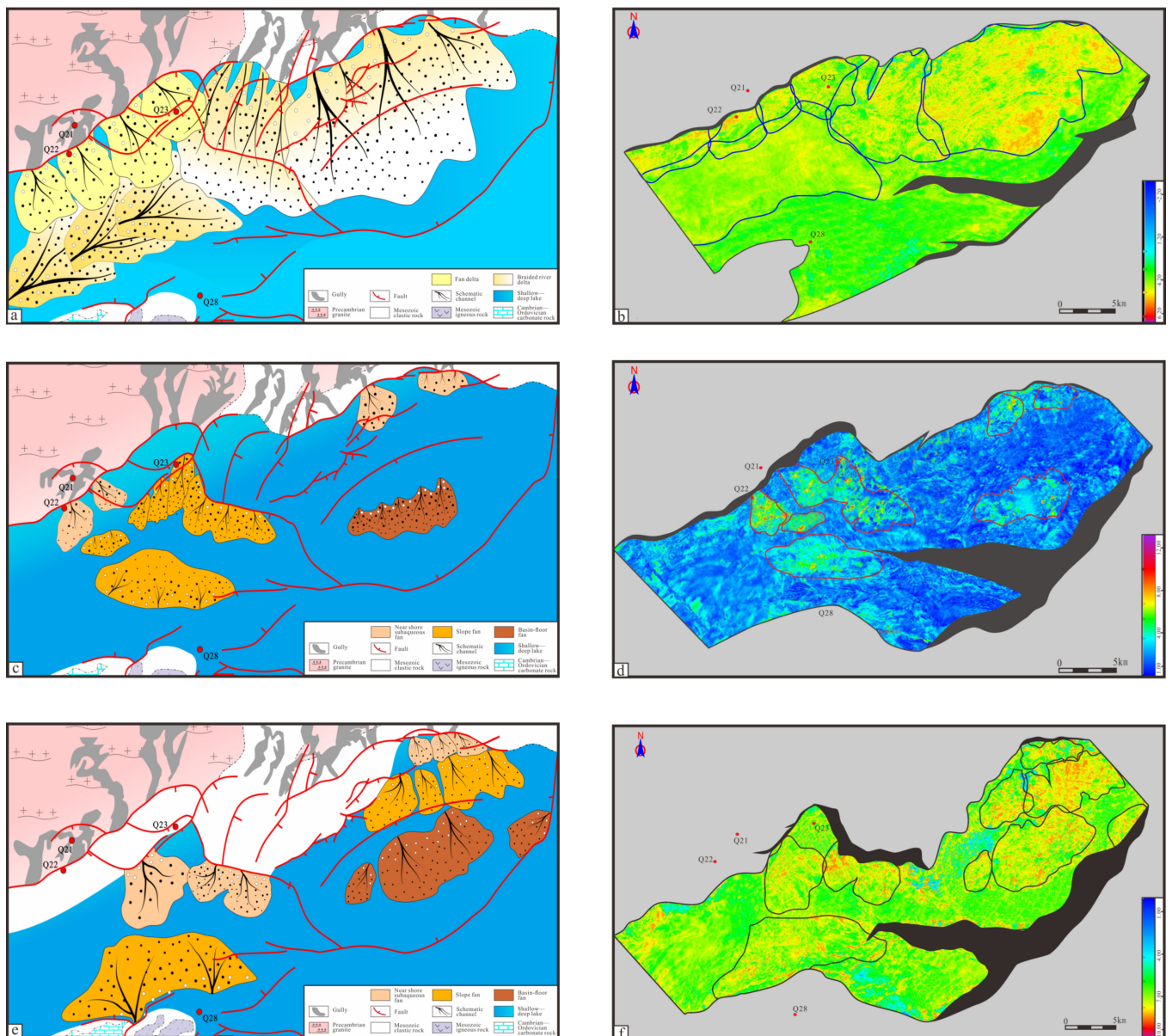
Figure 10. Sedimentary facies distribution and interpretative seismic amplitude extraction maps of the Es$_3$ in Qinnan depression. (**a**) The distribution of sedimentary facies in the HST of the Es$_{3U}$ sequence. (**b**) Seismic maximum-peak amplitude extraction maps corresponding to the distribution of delta deposition in the HST of the Es$_{3U}$ sequence. (**c**) The distribution of sedimentary facies in the LST and TST of the Es$_{3U}$ sequence. (**d**) Seismic maximum-peak amplitude extraction maps corresponding to the distribution of subaqueous gravity flow deposition in the LST and TST of the Es$_{3U}$ sequence. (**e**) The distribution of sedimentary facies in the Es$_{3L}$ sequence. (**f**) Seismic maximum-peak amplitude extraction maps corresponding to the distribution of subaqueous gravity flow deposition in the Es$_{3L}$ sequence.

5. Discussion

5.1. Advantages

The CAIM method can resolve the difficulty in accurately defining the sedimentary characteristics and distributions with inadequate data attained during reservoir exploration. Exploiting the compatible geological model established through the analysis of paleogeomorphology and the stratigraphic framework to conduct seismic interpretation,

the CAIM method allows for the geological analysis and geophysical analysis to complement each other.

With geological principles added to the process of geophysical analysis, the error rate of the analysis results is reduced. The geological analysis centering on the interpretation of the seismic data can be viewed as non-digital seismic inversion, which provides a novel graphical analysis route for geophysical analysis. Meanwhile, the utilization of seismic forward modeling (geophysical analysis) as a supplement to the geological analysis can achieve the digitalization of geological analysis, by which the correctness and uniqueness of the geological analysis results are ensured.

In addition, the CAIM method exhibits a wide range of applicability. On the one hand, the four sections of the method, i.e., paleogeomorphology construction, stratigraphic pattern analysis, seismic data interpretation and seismic forward modeling, have all been widely applied to the exploration and development of oil and gas in basins, which proves that there is little restriction to the application of the CAIM method. On the other hand, this method can be utilized when there are only 2D seismic data obtained, which reduces the dependence on data acquisition. It is worth noting that the obtainment of rocky *P*-wave velocities in a basin lacking wells is regarded as a main difficulty for the utilization of the CAIM method. In basins short of wells, a sedimentary velocity model can be established based on the measured *P*-wave velocities of the outcrop [37].

It is also interesting that the CAIM method features strong inclusiveness. During the process of seismic interpretation, not only can seismic facies and amplitude mentioned in this paper be used, but multiple seismic parameters can also be exploited. In fact, all interpretation methods of seismic data can be included in this method to facilitate the recognition of sedimentary characteristics and distributions.

All in all, the CAIM method, with a wide range of applicability and strong inclusiveness, combines geophysical analysis with geological analysis, which retains the role of geology in the process of geophysical analysis and eliminates the uncertainty and subjective effects of the results obtained via geological analysis alone.

5.2. Differences from Other Methods

Compared with other methods, the CAIM method highlights a closed-loop workflow and innovatively combines geological analysis and geophysics analysis so that the accuracy of the recognition of sedimentary characteristics and distributions in a basin with few or no wells is increased, and the success rate of reservoir exploration is greatly improved.

Many methods have been used to define sedimentary characteristics and distributions for reservoir exploration, which can be roughly divided into five categories: (1) geological analysis based on sedimentology, sequence stratigraphy and seismic sedimentology, which includes core or outcrop observation, a comprehensive analysis of seismic facies and log facies and an analysis of the source-to-sink system centering on lithology and geomorphology [51–53]; (2) geophysical analysis, which contains seismic forward modeling, seismic inversion and the reprocessing of seismic data [11]; (3) geochemical analysis including elemental analysis and organic geochemical analysis [47,49]; (4) hybrid analysis, which assembles results derived from different methods to acquire a comprehensive result [8,11,16,53]; and (5) the artificial intelligent method, which is used to conduct a comprehensive data analysis based on a large database [11]. Although the methods above have each their own advantages, they rarely have a closed-loop research process to ensure the correctness and uniqueness of the analysis results. By contrast, the closed-loop workflow of the CAIM method allows for the results of geological analysis and geophysical analysis to verify each other and ensures the correctness of the results. Additionally, as opposed to other methods that require a lot of logging data or experimental data, the application of the CAIM method can tap into only 2D seismic sections and rocky Vp at different depths to complete the study. Therefore, the CAIM method can be applied to study areas with few wells for the exploration of potential reservoirs.

5.3. Significances

This study not only introduces the CAIM method by elaborating on its principle, workflow and technologies, but also applies the method to explore potential reservoirs in the Es$_3$ of the Qinnan depression. The sedimentary characteristics and distributions defined via the CAIM method imply the distribution of potential reservoirs and, in turn, promote the exploration of oil and gas reservoirs in the Es$_3$ of the Qinnan depression.

Since the development of mudstone caprocks is a necessary condition for the accumulation of oil and gas and the deposition in the Es$_3$ of the Qinnan depression features a high sandstone proportion (Figure 10), sandstones in the Es$_{3L}$ and in the LST and TST of the Es$_{3U}$ under the MFS are deemed as potential reservoirs. And based on the sedimentary distribution in transgressive sequences, the potential reservoirs are inferred to distribute along slope break belts. The average *P*-wave velocity of sand-rich sedimentary bodies is lower than that of muddy sediments at the pinch-out sites, which implies the development of lithologic pinch-out hydrocarbon reservoirs.

Overall, the sedimentary characteristics and distributions in the Es$_3$ of the Qinnan depression indicate that sand-rich near-shore fan deposition, slope fan deposition and basin-floor fan deposition are potential reservoirs, of which the distribution is controlled by local accommodation change induced by the development of slope break belts.

6. Conclusions

Exhibiting a wide range of applicability and strong inclusiveness, the CAIM method, with a closed-up workflow, consists of paleogeomorphology construction, stratigraphic pattern analysis, seismic data interpretation and seismic forwarding modeling. The application of the CAIM method is of great significance for the studies on basins with little drilling data attained in the early exploratory stage, and can ensure the validity of the study results.

The sedimentary characteristics and distributions in the Es$_3$ of the Qinnan depression are defined through the CAIM method. The study results show that the deposition with a high proportion of sandstone in the study area is composed of braided river deltas and fan deltas in the HST as well as subaqueous gravity flow deposition (near-shore subaqueous fans, slope fans and basin-floor fans) in the LST and TST sequences. The fan deltas and braided river deltas develop in the western sag with a steep slope, and develop in eastern sag with a gentle slope, respectively. The distribution of near-shore subaqueous fans, slope fans and basin-floor fans are, respectively, delimited by the first-order, second-order and third-order slope break belts. And the results suggest that sand-rich subaqueous gravity flow depositions are the potential reservoirs.

References

1. Lu, Z.; He, Z.; Ma, S.; He, Y. Sedimentary characteristics and sand-body distributions in the Lower Permian He 8 Member, Ordos Basin, China. *Interpretation* **2022**, *10*, 223–236. [CrossRef]
2. Leila, M.; Yasser, A.; El Bastawesy, M.; El Mahmoudi, A. Seismic stratigraphy, sedimentary facies analysis and reservoir characteristics of the Middle Jurassic syn-rift sediments in Salam Oil Field, north Western Desert, Egypt. *Mar. Petrol. Geol.* **2022**, *136*, 105466. [CrossRef]
3. Yina, Z.; Wenjie, C.; Songling, Y.; Ke, Z.; Jingyang, C. Sedimentary characteristics of the Jurassic shelf-edge delta and oil and gas exploration in the Papuan Basin. *Earth Sci. Front.* **2021**, *28*, 167–176.
4. Cheng, Z.; Xu, H.; Wang, D.; Zhang, L.; Shi, Y.; Lu, Z.; Zhao, X. Research on sedimentary facies of Guantao Formation in Shanjiasi area of Dongying depression, China. *Energy Rep.* **2021**, *7*, 822–841. [CrossRef]
5. Xu, X.; Liu, L.; Li, X.; Yang, W.; Cao, Y.; Ma, H.; He, A.; Wang, R.; Leng, H.; Zhu, Y.; et al. Sequence stratigraphy, sedimentary characteristics of barrier coastal sedimentary system of the Benxi Formation (Gaoqiao area, Ordos basin) and favorable reservoir distribution. *Energy Rep.* **2021**, *7*, 5316–5329. [CrossRef]
6. Dalhoff, F.; Chalmers, J.A.; Gregersen, U.; Nohr-Hansen, H.; Rasmussen, J.A.; Sheldon, E. Mapping and facies analysis of Paleocene-Mid-Eocene seismic sequences, offshore southern West Greenland. *Mar. Petrol. Geol.* **2003**, *20*, 935. [CrossRef]
7. Sangree, J.B.; Widmier, J.M.; Payton, C.E. Seismic stratigraphy and global changes of sea level; Part 9, Seismic interpretation of clastic depositional facies. *AAPG Bull.* **1978**, *62*, 165–184.
8. Brown, L.F.; Fisher, W.L.; Payton, C.E. Seismic-stratigraphic interpretation of depositional systems; examples from Brazilian rift and pull-apart basins. In *Seismic Stratigraphy—Applications to Hydrocarbon Exploration*; Payton, C.E., Ed.; American Association of Petroleum Geologists: Tulsa, OK, USA, 1997; Volume 26, pp. 213–248.
9. Posamentier, H.W.; Kolla, V. Seismic geomorphology and stratigraphy of depositional elements in deep-water settings. *J. Sediment. Res.* **2003**, *73*, 367–388. [CrossRef]
10. Brown, A.R. *Interpretation of Three-Dimensional Seismic Data*; American Association of Petroleum Geologists: Tulsa, OK, USA, 2011; pp. 1–309.
11. Xu, G.; Haq, B.U. Seismic facies analysis: Past, present and future. *Earth-Sci. Rev.* **2022**, *224*, 103876. [CrossRef]
12. Posamentier, H. Seismic Geomorphology and Depositional Systems of Deep-Water Environments; Observations from Offshore Nigeria, Gulf of Mexico, and Indonesia. In Proceedings of the AAPG Annual Convention Program, Florence, Italy, 27 May 2002.
13. Yu, T.; Liu, H.; Liu, B.; Tang, S.; Tang, Y.; Yin, C. Restoration of karst paleogeomorphology and its significance in petroleum geology—Using the top of the Middle Triassic Leikoupo Formation in the northwestern Sichuan Basin as an example. *J. Petrol. Sci. Eng.* **2022**, *208*, 109638. [CrossRef]
14. Cheng, Y.F.; Dong, Y.L.D.; Zhu, X.M.; Yang, D.Q.; Wu, W.; Yang, K.; Su, B.; Zhao, R.X.; Qiao, C.K. Cretaceous paleogeomorphology restoration and its controlling mechanism on sand-bodies in Chunguang exploration area, Junggar Basin. *J. Palaeogeogr.* **2020**, *6*, 1127–1142.
15. Vail, P.R.; Audemard, F.; Bowman, S.A.; Eisner, P.N.; Perez-Cruz, G. *The Stratigraphic Signatures of Tectonics, Eustacy and Sedimentology: An Overview*; Einsele, G., Ricken, W., Seilacher, A., Eds.; Springer: Berlin/Heidelberg, Germany, 1991; pp. 617–659.
16. Leila, M.; Moscariello, A. Seismic stratigraphy and sedimentary facies analysis of the pre- and syn-Messinain salinity crisis sequences, onshore Nile Delta, Egypt: Implications for reservoir quality prediction. *Mar. Petrol. Geol.* **2019**, *101*, 303–321. [CrossRef]
17. Cai, Q.; Hu, M.; Ngia, N.R.; Hu, Z. Sequence stratigraphy, sedimentary systems and implications for hydrocarbon exploration in the northern Xujiaweizi Fault Depression, Songliao Basin, NE China. *J. Petrol. Sci. Eng.* **2017**, *152*, 471–494. [CrossRef]
18. Zimmer, E.H.; Howell, J.A.; Schofield, N.; Gawthorpe, R.L. Seismic geomorphology linked to sequence stratigraphy of an Eocene delta in the Outer Moray Firth, UKCS. *Mar. Petrol. Geol.* **2019**, *104*, 150–167. [CrossRef]
19. Batchelor, C.L.; Dowdeswell, J.A.; Pietras, J.T. Seismic stratigraphy, sedimentary architecture and palaeo-glaciology of the Mackenzie Trough: Evidence for two Quaternary ice advances and limited fan development on the western Canadian Beaufort Sea margin. *Quat. Sci. Rev.* **2013**, *65*, 73–87. [CrossRef]
20. Catuneanu, O.; Abreu, V.; Bhattacharya, J.P.; Blum, M.D.; Dalrymple, R.W.; Eriksson, P.G.; Fielding, C.R.; Fisher, W.L.; Galloway, W.E.; Gibling, M.R.; et al. Towards the standardization of sequence stratigraphy. *Earth-Sci. Rev.* **2009**, *92*, 102991. [CrossRef]
21. Matenco, L.C.; Haq, B.U. Multi-scale depositional successions in tectonic settings. *Earth-Sci. Rev.* **2020**, *200*, 102991. [CrossRef]
22. Catuneanu, O. Model-independent sequence stratigraphy. *Earth-Sci. Rev.* **2019**, *188*, 312–388. [CrossRef]
23. Xu, G.; Zhang, L.; Pang, X.; Chen, M.; Xu, S.; Liu, B.; Zuo, Y.; Luo, S.; Hu, L.; Chen, H.; et al. New method for the reconstruction of sedimentary systems including lithofacies, environments, and flow paths: A case study of the Xisha Trough Basin, South China Sea. *Mar. Petrol. Geol.* **2021**, *133*, 105268. [CrossRef]
24. Miall, A.D. *Stratigraphy: A Modern Synthesis*; Springer International Publishing: Cham, Switzerland, 2016; pp. 1–442.
25. Chopra, S.; Marfurt, K.J. Evolution of seismic interpretation during the last three decades. *Lead. Edge* **2012**, *31*, 654–676. [CrossRef]
26. Coléou, T.; Poupon, M.; Azbel, K. Unsupervised seismic facies classification: A review and comparison of techniques and implementation. *Lead. Edge* **2003**, *22*, 942–953. [CrossRef]
27. Song, C.; Liu, Z.; Wang, Y.; Li, X.; Hu, G. Multi-waveform classification for seismic facies analysis. *Comput. Geosci.* **2017**, *101*, 1–9. [CrossRef]

28. Ao, Y.; Li, H.; Zhu, L.; Ali, S.; Yang, Z. Identifying channel sand-body from multiple seismic attributes with an improved random forest algorithm. *J. Petrol. Sci. Eng.* **2019**, *173*, 781–792. [CrossRef]

29. Kumar, P.C.; Omosanya, K.O.; Sain, K. Sill Cube: An automated approach for the interpretation of magmatic sill complexes on seismic reflection data. *Mar. Petrol. Geol.* **2019**, *100*, 60–84. [CrossRef]

30. Zeng, H. Frequency-dependent seismic-stratigraphic and fades interpretation. *AAPG Bull.* **2013**, *97*, 201–221. [CrossRef]

31. Xie, T.; Zheng, X.; Zhang, Y. Seismic facies analysis based on speech recognition feature parameters. *Geophysics* **2017**, *82*, 23–35. [CrossRef]

32. Farzadi, P. Seismic facies analysis based on 3D multi-attribute volume classification Dariyan Formation, SE Persian Gulf. *J. Petrol. Geol.* **2006**, *29*, 159–173. [CrossRef]

33. Di, H.; Alfarraj, M.; AlRegib, G. Three-dimensional curvature analysis of seismic waveforms and its interpretational implications. *Geophys. Prospect.* **2019**, *67*, 265–281. [CrossRef]

34. Johansen, S.E.; Arntsen, B.; Raknes, E.B.; Omosanya, K.O.L.; Harishidayat, D.; Henningsen, T. Seismic forward modelling of the Kvalhovden outcrop, Spitsbergen, Norway. *Mar. Petrol. Geol.* **2023**, *147*, 106000. [CrossRef]

35. Shang, W.; Xu, S.; Li, X.; Liang, F.; Wu, C.; Wang, J.; Li, Z.; Sun, Y.; Li, Y.; Li, M.; et al. Utilizing 2D seismic forward modeling to constrain the seismic response and plane distribution of grain shoal reservoir in the northern slope of Central Sichuan Paleo-uplift, Sichuan Basin. *Mar. Petrol. Geol.* **2023**, *152*, 106228. [CrossRef]

36. Tomassi, A.; Trippetta, F.; de Franco, R.; Ruggieri, R. From petrophysical properties to forward-seismic modeling of facies heterogeneity in the carbonate realm (Majella Massif, central Italy). *J. Petrol. Sci. Eng.* **2022**, *211*, 110242. [CrossRef]

37. Xiong, R.; Zheng, J.; Wang, X.; Huang, L.; Guo, L. 3D Outcrop geologic modeling and seismic forward modeling of mound-beach complexes. *Arab. J. Geosci.* **2022**, *15*, 1289. [CrossRef]

38. Wan, L.; Hurter, S.; Bianchi, V.; Li, P.; Wang, J.; Salles, T. The roles and seismic expressions of turbidites and mass transport deposits using stratigraphic forward modeling and seismic forward modeling. *J. Asian Earth Sci.* **2022**, *232*, 105110. [CrossRef]

39. Grasseau, N.; Grélaud, C.; López-Blanco, M.; Razin, P. Forward seismic modeling as a guide improving detailed seismic interpretation of deltaic systems: Example of the Eocene Sobrarbe delta outcrop (South-Pyrenean foreland basin, Spain), as a reference to the analogous subsurface Albian-Cenomanian Torok-Nanushuk Delta of the Colville Basin (NPRA, USA). *Mar. Petrol. Geol.* **2019**, *100*, 225–245.

40. Shuster, M.W.; Aigner, T. Two-dimensional synthetic seismic and log cross sections from stratigraphic forward models. *AAPG Bull.* **1994**, *78*, 409–431.

41. Wang, D.; Yu, H.; Wang, J.; Li, R.; Li, L. Key exploration techniques for stratigraphic-lithologic reservoirs and their application in Qinnan sag, Bohai sea. *China Offshore Oil Gas* **2015**, *27*, 16–24. (In Chinese with English Abstract)

42. Lai, W.; Xu, C.; Wang, X.; Wang, C.; Liu, F. A study on Paleogene sequence stratigraphy and sedimentary systems and a discussion on hydrocarbon exploration directions in Qinnan depression. *China Offshore Oil Gas* **2007**, *5*, 300–305. (In Chinese with English Abstract)

43. Cai, S.; Zhou, D.; Wang, D.; Zhang, J.; Zhang, Z.; Li, Y. Tectonic development characteristics and favorable exploration direction of Qinnan sag in Bohai Bay Basin. *Acta Petrol. Sin.* **2019**, *40*, 532–541. (In Chinese with English Abstract)

44. Zhang, Z.; Xu, C.; Guo, R.; Li, L.; Yang, C. Cenozoic fault system and tectonic evolution of Qinan Sag in Bohai Sea. *Fault-Block Oil Gas Field* **2019**, *26*, 158–161+167. (In Chinese with English Abstract)

45. Cai, S.; Lü, D.; He, D.; Zhang, J.; Yu, Y. Characteristics of tectonic migration in Qinnan sag of the Bohai Bay Basin and its impact on hydrocarbon accumulation. *Acta Petrol. Sin.* **2019**, *40* (Suppl. 2), 67–78. (In Chinese with English Abstract)

46. Liu, H. Study on the Paleogene system Formation Sequence stratigraphy and depositional system in Qinnan depression of Bohai sea. Master's Thesis, Chengdu University of Technology, Sichuan, China, 2014. (In Chinese with English Abstract).

47. Wang, Q.; Hao, F.; Xu, C.; Zhu, Y.; Sun, Z.; Zou, H. The origin and charging directions of Neogene biodegraded oils: A geochemical study of large oil fields in the middle of the Shijiutuo Uplift, Bohai Sea, China. *Mar. Petrol. Geol.* **2017**, *88*, 200–213. [CrossRef]

48. Zhao, J.; Liu, C.; Huang, L.; Mountney, N.; Han, S.; Liu, P.; Hu, J. Original Sedimentary Pattern of an Inverted Basin: A Case Study from the Bozhong Depression, Offshore Bohai Bay Basin. *Acta Geol. Sin.* **2016**, *90*, 2163–2181. [CrossRef]

49. Yang, C.; Guo, R.; Wang, F.; Zhang, Z.; Pei, X. Quantitative prediction of TOC in source rocks of the Member 3 of Shahejie Formation in Qinnan Depression, Bohai sea, China. *J. Chengdu Univ. Technol. (Sci. Technol.)* **2019**, *46*, 549–557. (In Chinese with English Abstract)

50. Veeken, P.C.H.; Moerkerken, B.V. *Seismic Stratigraphy and Depositional Facies Models*; Academic Press: Amsterdam, The Netherlands, 2013; pp. 15–410.

51. Xu, C.G.; Du, X.F.; Zhu, H.T. *Sand Control Principle and Application of Source to Sink System in Continental Rift Basin*; China Science Publishing and Media Ltd.: Beijing, China, 2020; pp. 27–54.

52. Huang, C.; Wang, H.; Wu, Y.; Wang, J.; Chen, S.; Ren, P.; Liao, Y.; Zhao, S.; Xia, C. Genetic types and sequence stratigraphy models of Palaeogene slope break belts in Qikou Sag, Huanghua Depression, Bohai Bay Basin, Eastern China. *Sediment. Geol.* **2012**, *261–262*, 65–75. [CrossRef]

53. Wang, C.C.; Xu, G.Q.; Zhuo, Y.H. *Fundamental for Seismic-Geologic Interpretation (Chinese and English Edition)*; Petroleum Industry Press: Beijing, China, 2015; p. 126.